Article

Rational design of a red-emissive fluorophore with AIE and ESIPT characteristics and its application in light-up sensing of esterase

Lu Peng, Shidang Xu, Xiaokun Zheng, Xiamin Cheng, Ruoyu Zhang, Jie Liu, Bin Liu, and Aijun Tong

Anal. Chem., **Just Accepted Manuscript** • DOI: 10.1021/acs.analchem.6b04974 • Publication Date (Web): 03 Feb 2017

Rational design of a red-emissive fluorophore with AIE and ESIPT characteristics and its application in light-up sensing of esterase

Lu Peng,[†,‡] Shidang Xu,[‡] Xiaokun Zheng,[†] Xiamin Cheng,[‡] Ruoyu Zhang,[‡] Jie Liu,[‡] Bin Liu*[,‡,§] and Aijun Tong*[,†]

[†]Department of Chemistry, Beijing Key Laboratory for Analytical Methods and Instrumentation, Key Laboratory of Bioorganic Phosphorus Chemistry and Chemical Biology, Tsinghua University, Beijing 100084, People' s Republic of China. Fax: +86-10-62787682. Email: tongaj@mail.tsinghua.edu.cn.

[‡]Department of Chemical and Biomolecular Engineering, National University of Singapore, 4 Engineering Drive 4, Singapore 117585, Singapore. Fax: +65-67791936. E-mail: cheliub@nus.edu.sg.

[§]Institute of Materials Research and Engineering (A*STAR), 3 Research Link, Singapore 117602, Singapore

ABSTRACT: The development of red fluorophores with efficient solid-state emission is still challenging. Herein, a red fluorophore **1** with aggregation-induced emission (AIE) and excited-state intramolecular proton transfer (ESIPT) characteristics is rationally designed and facilely synthesized by attaching an electron donor diethylamine and an electron acceptor maleonitrile group to salicyladazine. In contrast to many red fluorophores which undergo serious aggregation-caused quenching (ACQ), compound **1** emits bright red fluorescence (λ_{em} = 650 nm, Φ_F = 24.3%) in the solid state with a large Stokes shift of 174 nm. Interestingly, control compounds **2** and **3**, which have similar structures as **1**, exhibit obvious aggregation-caused quenching (ACQ) characteristics. The difference in the crystal structures of **1**, **2** and **3** reveals that the interplanar spacing among molecules plays a decisive role in realizing the AIE characteristics of **1**. Moreover, when the hydroxyl group of **1** was substituted by an esterase reactive acetoxyl, a fluorescence light-up probe **4** was developed for sensing of esterase based on the selective reaction between **4** and esterase to generate the AIE and ESIPT active molecule **1**. The linear range for in vitro quantification of esterase is 0.01-0.15 U/mL with a detection limit of 0.005 U/mL. Probe **4** was also successfully applied to image esterase in mitochondria of living cells.

Fluorescence detection of various analytes has received much research interest because of its advantages such as low cost, simplicity, good sensitivity, and capability of real-time and non-destructive bio-imaging[1-8]. Among all the luminescent molecules, red fluorophores play a crucial role in fluorescence detection and bio-imaging because they could minimize photo-damage to living cells, enable deep tissue penetration and overcome the interference from biological background fluorescence[9-12]. However, most fluorophores have bright emission in the solution state, but their luminescence declines obviously in the aggregated state, which is known as aggregation-caused quenching (ACQ)[13, 14]. The situation is even worse for red fluorophores because most of them contain large aromatic rings which could form strong intermolecular π-π interactions[15, 16], to cause non-radiative decay in the aggregated state.

Fluorophores with aggregation-induced emission (AIE)[17-22] properties are an emerging class of molecules displaying strong fluorescence in their solid or aggregate states. So far, many AIE fluorophores based on hydrocarbons, heteroatoms or organometallics have been constructed as fluorescent materials for biomedical applications[23-27]. Although fluorophores with both red fluorescence and AIE characteristics are more preferable, unfortunately, limited red AIE fluorophores have been reported[28-33]. The scarcity of red AIE fluorophore is mainly due to the difficulty of molecular design and structural modifications. To design red AIE fluorophores, one has to consider either increasing the molecular conjugation length, or selecting a proper combination of an electron donor and an acceptor to red-shift the emission. Researchers often encounter a dilemma because this strategy may usually lead to ACQ characteristics[34, 35]. In addition, in many cases, twisted molecular structures are needed to acquire AIE properties, which makes the design and synthesis of red AIE fluorophores even more difficult.

Previously, we have developed one class of AIE-active fluorophores[36, 37] which is based on the excited state intramolecular proton transfer (ESIPT)[38, 39] mechanism. For these fluorophores, twisted structure is not necessary to exhibit AIE characteristics, while the hydroxyl groups are responsible for ESIPT and essential for their AIE characteristics in aggregate and solid states. Once the hydroxyl group is blocked, the fluorescence of the molecule will be quenched or changed to a different wavelength. This brings the advantages of facile synthesis and ease of chemical modifications for the development of various light-up probes[40, 41]. However, the limitations of the ESIPT dyes include the short absorption (λ_{abs} < 400 nm) and emission wavelengths (λ_{em} < 600 nm), which does not match well with the excitation of confocal microscope (≥ 405 nm). Herein, we rationally developed a fluorophore **1** with both red fluorescence and AIE characteristics based on salicyladazine (Scheme 1a). Red fluorescence is achieved by attaching an electron donor diethylamine and an electron acceptor maleonitrile group to salicyladazine. Meanwhile, **1** maintains the hydroxyl group to keep AIE and ESIPT characteristics. More importantly, the proper crystal packing pattern of **1**, which makes the intermolecular π-π interactions very weak, prevents the non-radiative decay of excited electrons and allows **1** to show good red emission property (λ_{em} = 650 nm, Φ_F = 24.3%) in the solid state. Apart from the red fluorescence, **1** possesses appropriate absorption band (λ_{abs} = 437 nm in solution state

and 476 nm in solid state) for confocal imaging with a large Stokes shift, which greatly reduces self-quenching of fluorescence.

A light-up probe **4** for esterase based on **1** was also developed through blocking the hydroxyl group of **1** with an esterase selective acetoxyl group[42, 43] (Sheme 1b). Esterase was selected as the model target because esterase is an important drug target[44, 45] and prodrug activator[46]. After **4** was reacted with esterase, **1** was expected to be regenerated to show both AIE and ESIPT characteristics. Although several fluorescent probes[42, 43, 47, 48] have been developed for esterase, they are not able to selectively image esterase in a specific organelle of cells. Moreover, they suffer from disadvantages such as ACQ when accumlated in cells and small Stokes shifts (< 40 nm)[42, 43]. Previously, we have reported a light-up probe[49] based on AIE and ESIPT characteristics for specific detection of lysosomal esterase, which emits green fluorescence (λ_{em} = 532 nm). Considering that a red fluorescent probe with AIE and ESIPT characteristics would be more suitable for bio-imaging, probe **4** was developed in this work. **4** showed red light-up fluorescence and high specificity to esterase. Moreover, it was found to be accumulated in mitochondria of living cells and emit bright red fluorescence even in the aggregated state. Because mitochondria plays critical roles in many vital cellular processes, such as ATP production, central metabolism and apoptosis[50, 51], probe **4** might find promising potential in the biological study of esterase.

Scheme 1. (a) Chemical structures of compound 1, 2, 3 and corresponding photographs of their solids without or with a UV lamp at 365 nm. (b) The fluorescent light-up probe 4 for sensing of esterase.

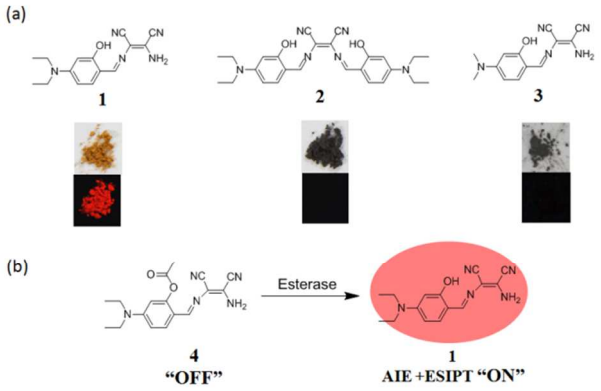

EXPERIMENTAL SECTION

Synthesis of 1. In 50 mL of ethanol, 4-(diethylamino)salicylaldehyde (1.93 g, 10 mmol) and diaminomaleonitrile (1.08 g, 10 mmol) were added. After being stirred at r.t. for 7 days, the product was precipitated as brown solid. The product was filtrated under vacuum, washed by ethanol and dried under vacuum to afford pure product of **1** (2.31 g, 8.2 mmol, 82% yield). ^{1}H NMR (400 MHz, d_6-DMSO): δ = 10.55(s, 1H), 8.35(s, 1H), 7.60 (d, 1H, J = 12.0 Hz), 7.33(s, 2H), 6.21 (dd, 1H, J_1 = 8.0 Hz, J_2 = 8.0 Hz), 6.10 (d, 1H, J = 4 Hz), 3.39 (dd, 4H, J_1 = 16.0 Hz, J_2 = 16.0 Hz), 1.12 (t, 6H); ^{13}C NMR (400 MHz, d_6-DMSO): 161.12, 155.92, 152.29, 132.88, 123.00, 115.71, 114.76, 109.55, 105.31, 105.03, 97.14, 44.45, 31.13, 13.02 (2C). Mass spectrometry: calc. for $C_{15}H_{17}N_5NaO$ $[M+Na]^+$ 306.1, found 306.1 (ESI).

Synthesis of 2. In 50 mL of ethanol, 4-(diethylamino)salicylaldehyde (1.93 g, 10 mmol) and diaminomaleonitrile (0.50 g, 5 mmol) were added. The mixed solution was refluxed for 3 days, the product was precipitated as black solid. The product was filtrated under vacuum, washed by ethanol and dried under vacuum to afford pure product of **2** (1.71 g, 3.7 mmol, 75% yield). ^{1}H NMR (400 MHz, d_6-DMSO): δ = 8.57 (s, 2H), 7.57 (d, 2H, J = 11.4 Hz), 6.44 (d, 2H, J = 11.0 Hz), 6.16 (s, 2H), 4.47 (t, 8H), 1.15 (t, 12H). Solid-state ^{13}C NMR (600 MHz): 166.64, 165.72, 163.42, 161.82, 156.30, 154.00, 137.53 (2C), 123.06, 121.52, 111.57 (2C), 110.26 (2C), 107.43 (2C), 98.62, 97.24, 48.91 (2C), 47.38 (2C), 15.89 (2C), 14.29 (2C).

Synthesis of 3. In 50 mL of ethanol, 4-(dimethylamino)salicylaldehyde (1.93 g, 10 mmol) and diaminomaleonitrile (1.08 g, 10 mmol) were added. The mixed solution was stired at r.t. for 7 days, the product was precipitated as black solid. The product was filtrated under vacuum, washed by ethanol and dried under vacuum to afford pure product of **3** (1.66 g, 6.5 mmol, 65% yield). ^{1}H NMR (400 MHz, d_6-DMSO): δ=10.58 (s, 1H), 8.37 (s, 1H),7.63 (d, 1H, J = 11.9 Hz),7.38 (s, 2H), 6.33 (d, 1H, J = 11.8 Hz), 6.11 (d, 1H, J = 3.2 Hz), 3.03 (q, 6H); ^{13}C NMR (400 MHz, d_6-DMSO): 160.82, 155.94, 154.65, 132.57, 123.35, 115.76, 114.85, 110.09, 105.46, 105.18, 97.84, 44.04 (2C). Mass spectrometry: calc. for $C_{13}H_{12}N_5O$ $[M-H]^-$ 254.1, found 254.1 (ESI).

Synthesis of 4. In 20 mL of acetonitrile, 4-(diethylamino)salicylaldehyde (0.725 g, 3.75 mmol), acetic anhydride (0.7 mL, 7.5 mmol) and cesium carbonate (1.225 g, 3.725 mmol) were added. The mixed solution was refluxed overnight and extracted three times using 30 mL of ethyl acetate, washed with brine solution, dried over anhydrous Na_2SO_4 and the solvent was evaporated to afford crude product of **5** (0.63 g, 2.7 mmol, 72% yield). **5** (0.62 g, 2.63 mmol) was further reacted with diaminomaleonitrile (0.284 g, 2.63 mmol) in 20 mL ethanol at r.t. for 5 days. The resulting precipitates were filtrated and washed three times with 30 mL of ethanol to yield **4** as brown powder (0.318 mg, 0.97 mmol, 37% yield). ^{1}H NMR (400 MHz, $CDCl_3$): δ= 8.32 (s, 1H), 7.88 (d, 1H, J = 12.36 Hz), 6.59 (d, 1H, J = 9.6 Hz), 6.33 (d, 1H, J = 2.32 Hz), 5.00 (s, 2H), 3.43 (t, 4H), 2.37 (t, 3H), 1.22 (t, 6H); ^{13}C NMR (400 MHz, $CDCl_3$): 169.75, 153.48 (2C), 152.01, 130.12, 122.17, 114.39, 114.22, 112.82, 110.19, 109.78, 104.56, 44.93 (2C), 21.11, 12.66 (2C). Mass spectrometry: calc. for $C_{17}H_{18}N_5O_2$ $[M-H]^-$ 324.1, found 324.1 (ESI).

Analytical procedures. The stock solution (1.0×10^{-2} M) of **4** was prepared in DMSO. Stock solutions of esterase (100 U/mL) and other analytes ($CaCl_2$, $Mg(NO_3)_2$, $Zn(NO_3)_2$, $Fe(NO_3)_3$, $Cu(NO_3)_2$, pepsin, lysozyme, cysteine, vitamin C, alanine, BSA) were prepared in distilled deionized water, respectively. In a typical detection, 10 μL of **4** stock solution was added into a test tube, which was diluted to 1.0 mL with PBS buffer (10 mM, pH 7.4). Subsequently, a proper amount of esterase stock solution was added. The fluorescence spectra were recorded before and after the addition of esterase at different time.

Cell imaging. MCF-7 and HeLa cells were seeded at a density of 2×10^4/well in the chamber (LAB-TEK, Chambered Cover glass System) and grown for 18 h at 37 ℃ in a humidified 5% CO_2 incubator. The cells were treated without or with the esterase inhibitor solution (AIEBSF, 10 mM) in PBS buffer (10 mM, pH 7.4) for 20 min at 37 ℃. After washing with PBS buffer to remove the remaining inhibitor, the cells were further incubated with

the solution of **4** (50 μM, DMSO:H_2O=5:995 v/v) for 10 min. The solution of **4** was prepared by adding 5 μL of its DMSO stock solution (10 mM) into a microtube, subsequently 995 μL Dulbecco's modified Eagle medium (DMEM) was added with vigorous mixing. The fluorescence imaging of the cells was collected using the red channel (λ_{ex}=405 nm, 547-647 nm). For co-localization imaging, HeLa cells were pre-stained with nucleus staining dye Hochest (10 mg/mL) or Mito-Tracker Green (100 nM) for 20 min and then incubated with **4** (50 μM) for 10 min. The images were collected using blue channel (λ_{ex} = 405 nm, λ_{em} = 420-480 nm), green channel (λ_{ex} = 488 nm, λ_{em} = 500-540 nm) and red channel (λ_{ex} = 405 nm, λ_{em} = 550-650 nm), respectively.

Scheme 2. Synthesis of compound (a) 1 , (b) 2, (c) 3 and (d) 4.

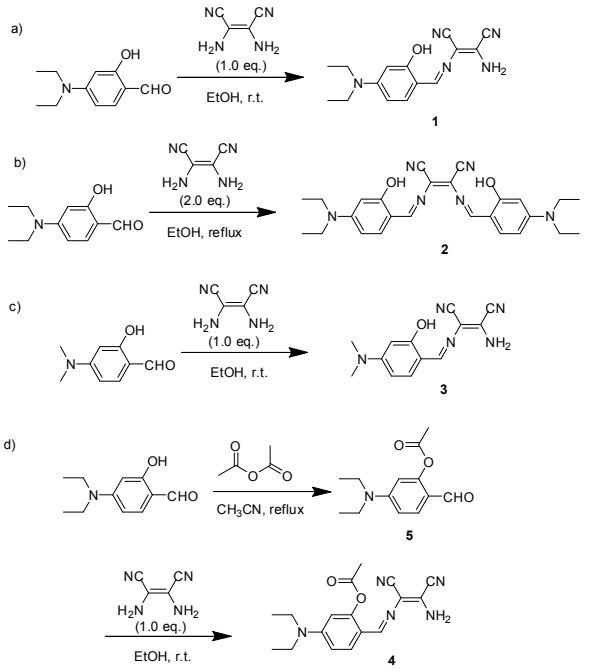

RESULTS AND DISCUSSION

Optical Properties. The solid state fluorescence of **1**, **2** and **3** was studied first to test our design principle. As shown in Scheme 1a and Figure 1a, powders of **1** emit strong red fluorescence (λ_{em} = 650 nm, Φ_F = 24.3%), while the powders of **2** and **3** display low fluorescence (Φ_F < 1.0%). This accords well with the absorption spectrum in solid state (Figure 1b) that **2** and **3** have strong absorption in visible region, which could cause serious self-quenching of their fluorescence.

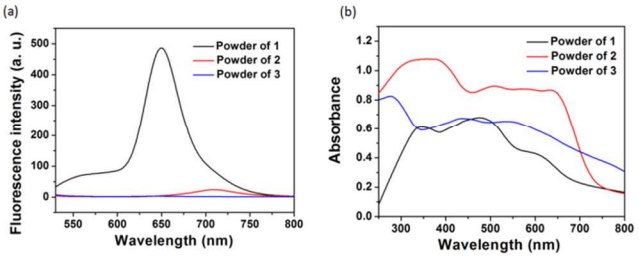

Figure 1. (a) Fluorescence and (b) absorption spectra of compound **1**, **2** and **3** in solid state. Excitation was set at 500 nm.

Furthermore, we studied the effect of water volume fraction on the fluorescence of **1**, **2** and **3**, respectively (Figures 2, S7 and S8). The fluorescence change of **1** was investigated in water/DMSO co-solvents with different water volume fractions (f_w = 0-90 vol%), and the results are shown in Figure 2. In a good solvent (f_w = 0 vol%), **1** disperses well and exhibits green fluorescence. Nevertheless, in a poor solvent (f_w = 90 vol%), an intense red fluorescence can be observed, suggesting **1** with AIE characteristics. The AIE effect of **1** occurs when the water volume fraction in the co-solvent is more than 70%. The intensity ratio (I_{619}/I_{513}) is enhanced at a higher water volume fraction, which correlates well with the increased aggregates formation in poorer solvents. Moreover, in the poor solvent (f_w = 90 vol%), a leveling-off in the visible region of its absorption spectra (commonly observed in nano-aggregate suspensions[52]) strongly suggests the formation of a poorly-soluble "aggregate" state (Figure S1a). The dynamic light scattering (DLS) analysis results of **1** indicate that the average particle diameter is 540.4 nm (Figure S2a).

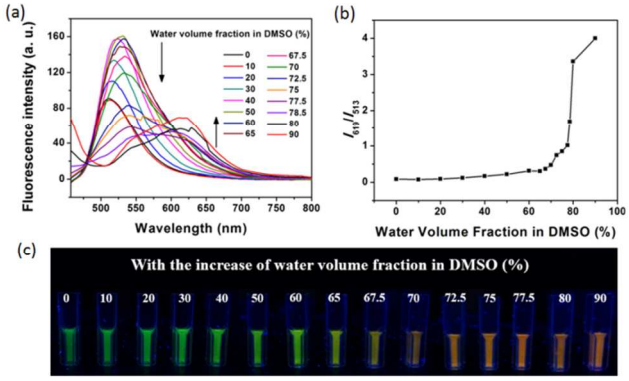

Figure 2. Effect of water volume fraction on the (a) fluorescence spectra and (b) ratio of intensity (I_{619}/I_{513}) of **1** (100 μM) in water/DMSO containing 10 mM PBS buffer at pH 7.4. Excitation was set at 437 nm. (c) The corresponding photographs of **1** with a UV lamp at 365 nm.

To further confirm that the green fluorescence of **1** was originated from the solution state while red fluorescence was from the aggregate state, the effects of concentration and pH on its fluorescence were investigated. As shown in Figure S3, **1** emits green fluorescence at low concentrations (0-2.0 mM), but red fluorescence at high concentrations (5.0-100.0 mM), suggesting that the green and red fluorescence are attributed to the solution and aggregate state, respectively. Moreover, **1** exhibits a significant fluorescence color change from red to green with an intensity ratio (I_{547}/I_{619}) enhanced when the pH is increased from 3.0 to 13.0 in aqueous solution (Figure S4). This accords with the fact that **1** forms aggregates in acidic condition because of poor solubility in water while it stays in solution state under alkaline condition because the deprotonation process can improve its solubility. In addition, the fluorescence lifetime of **1** (Figure S5) in a poor solvent (f_w = 90 vol%, τ = 2.6 ns) is comparable to that in solid state (τ = 3.2 ns), indicating the red fluorescence of **1** in the poor solvent is attributed to the aggregate state. On the other hand, the short fluorescence lifetime in a good solvent (f_w = 0 vol%, τ = 0.2 ns) is resulted from the non-radiative decay of excited electrons due to frequent intermolecular collision[53].

The red-shifted emission of fluorophores could arise from intramolecular charge transfer (ICT)[54, 55], which lowers the π-π* energy gap. To evaluate whether the red emission of **1** is caused by ICT or not, the effect of solvent polarity is studied

because solvatochromism is usually a strong evidence of the existence of ICT[56, 57]. However, as shown in Figure S6 and Table S1, the absorption and emission spectra do not change much with the increase of solvent polarity, confirming that ICT has little contribution to the red-shifted emission of **1**.

Interestingly, **2** and **3** were found to be with ACQ characteristics (Figures S7 and S8). **2** and **3** both dissolve well in DMSO but are not soluble in water. In DMSO (f_w = 0 vol%), **2** and **3** disperse well and exhibit red and green fluorescence, respectively. However, in a poor solvent (f_w = 90 vol%), little fluorescence could be observed. The fluorescence intensity was found to decrease at a higher water volume fraction, which correlates well with the increased aggregates formation in poorer solvents. The fluorescence intensity decrease of **2** in DMSO with its concentration increase also suggests its ACQ characteristics (Figure S9).

Crystal Analysis. To investigate the decisive factor that makes **1** AIE while **2** and **3** ACQ, we further studied the single crystal structure of **1**, **2** and **3** (Figure 3). In the crystals of **1**, molecules form effective J-aggregates. The ethyl groups result in increased steric hindrance between two adjacent molecules. The distance between the central benzene planes of adjacent molecules is 4.01 Å, which is greater than 3.80 Å and could impede intermolecular π-π interactions and thus avoid the quenching of fluorescence in either the solid state or aggregate state. Contrarily, in the crystals of **2**, molecules stack up in disorder. The molecular planes were twisted into an arch-like shape. The inter-planar spacing between two adjacent molecules is 3.25 Å, within the range of intermolecular π-π stacking. Although the ethyl groups are far from each other due to steric hindrance, the molecular plane is bent and the central benzene planes of adjacent molecules are much closer than those of **1**, thus making the intermolecular π-π interactions strong enough to quench the fluorescence in the solid and aggregate state. As for **3**, molecules adopt J-aggregate packing pattern, but the steric hindrance of methyl groups is too weak to prevent π-π interactions with an inter-planar spacing of 3.32 Å, resulting in its ACQ characteristics.

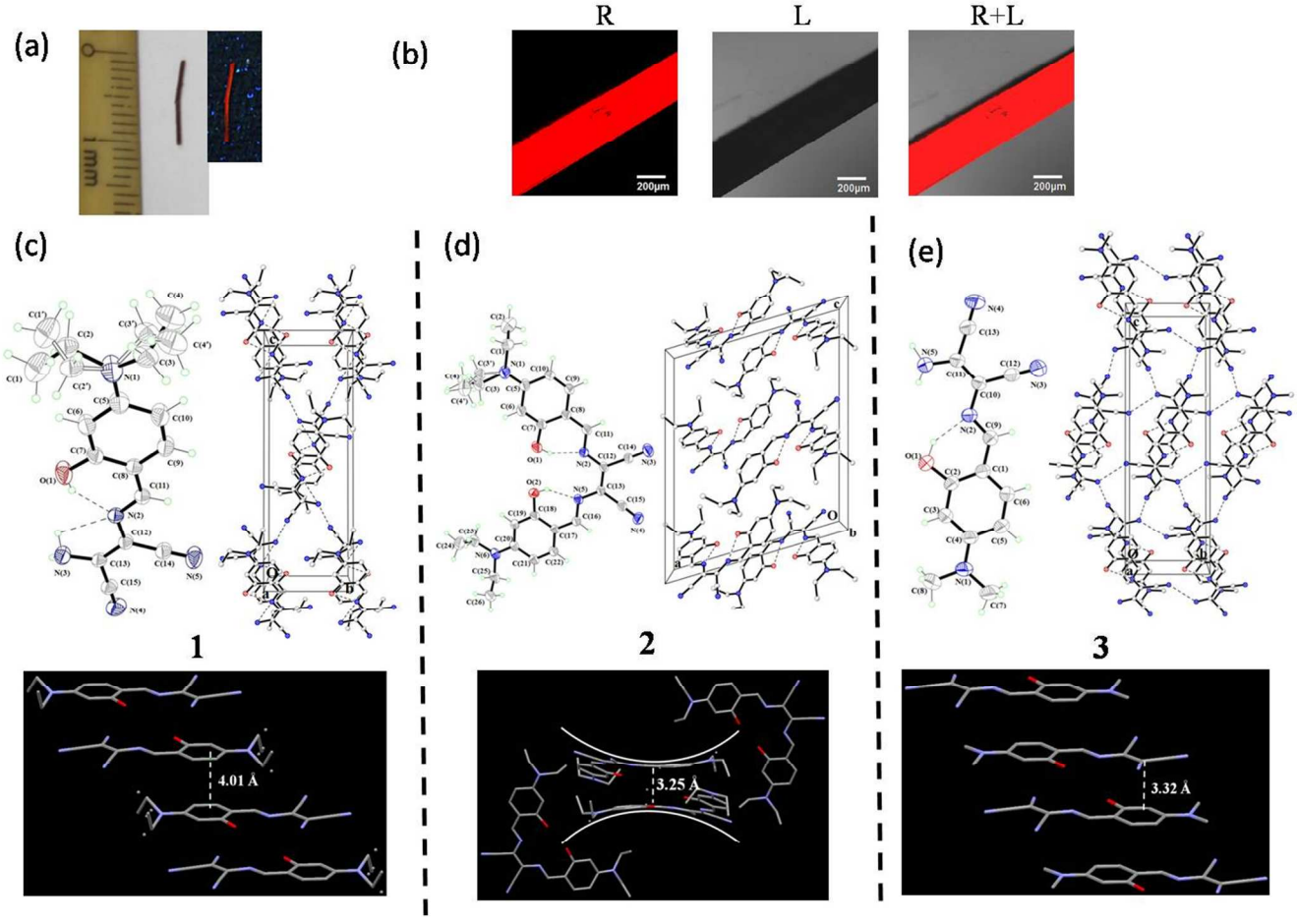

Figure 3. (a) Photographs of the single crystal of **1** without or with a UV lamp at 365 nm. (b) Confocal micrographs of the crystal of **1**. The excitation was set at 405 nm. "R", "L": red and bright channels, respectively. Red channel: 547-647 nm. (c-e) Single crystal analyses and packing patterns of **1**, **2** and **3**, respectively.

Light-up sensing of esterase. Compound **1** was further developed into a red light-up fluorescent probe **4** for sensing of esterase. The fluorescence of **4** in the absence and presence of esterase was studied to prove our design principle above (Scheme 1b). The blocked compound **4** displayed very weak fluorescence (Figure 4a), suggesting successful blocking effect of acetoxyl group. Upon addition of esterase, the fluorescence of **4** enhanced gradually until red fluorescence was observed. The time-dependent fluorescence intensity change of **4** was recorded without and with the addition of esterase (Figure 4b), showing that the fluorescence light-up effect only occurs in the presence of esterase. As shown in Figures 4c and 4d, a

good linearity was found in the esterase concentration range of 0.01-0.15 U/mL. The detection limit was calculated as 0.005 U/mL based on the definition by IUPAC ($C_{DL} = 3S_b/m$) from 10 blank solutions, which is similar to the previously reported probes[48].

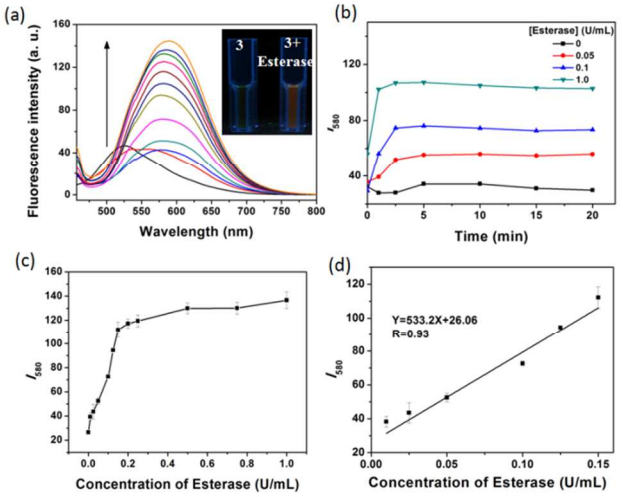

Figure 4. (a) Fluorescence spectra of **4** (100 μM) in the presence of various concentrations of esterase (0-1.0 U/mL) in 10 mM PBS buffer solution at pH 7.4, 37 ℃. Insets from left to right: photographs of **4** (100 mM) without or with esterase (1.0 U mL) under UV light (365 nm). (b) The corresponding fluorescence intensity (I_{580}) change over time and (c) concentration. (d) Calibration curve of the fluorescence intensities (I_{580}) versus esterase concentrations. The measurements in (c) and (d) were performed after the addition of esterase for 20 min.

It has been reported by Nagano's group[42] and others[43] that acetoxyl can be cleaved by esterase to release hydroxyl group. To verify this, the fluorescent product after reaction between probe **4** and the esterase was isolated by filtration and subsequently characterized. The results in Figure S10 clearly suggest the formation of **1** from **4**, supporting the hypothesis in our design (Scheme 1b). The selectivity of probe **4** towards esterase was also studied (Figure S11). No change was observed with some commonly used inorganic salts or biomolecules. Thus, probe **4** shows good selectivity to esterase. To confirm that the fluorescence enhancement was caused by esterase, the inhibition effect of 4-(2-aminoethyl)benzenesulfonyl fluoride (AIEBSF)[42] on esterase activity has been examined. As shown in Figure S12, the fluorescence intensity was weakened by the addition of AIEBSF, suggesting the mechanism of fluorescence enhancement by the enzymatic reaction between **4** and esterase.

Imaging esterase in living cells. To further demonstrate the potential of probe **4** to image esterase in living matrices, we carried out the experiments in living cells. After the cells were incubated with **4** (50 μM) for 10 min, strong fluorescence was exhibited (Figures 5b and S13). To demonstrate the specificity of **4** to esterase, a control experiment was undertaken (Figure 5c). Cells were pretreated with the inhibitor AIEBSF (10 mM), which was expected to inhibit the activity of esterase, and then incubated with probe **4**, a remarkable decrease in fluorescence intensity was observed. This confirms the specificity of probe **4** towards esterase over other analytes in living cells.

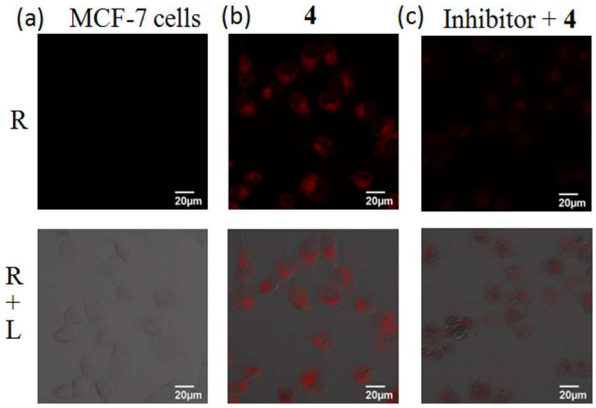

Figure 5. Imaging esterase in living MCF-7 cells. Cells (a) without or (b) with incubation of **4** (50 μM) for 10 min; (c) cells were pre-incubated with 10 mM inhibitor for 20 min and then treated with **4** (50 μM) for 10 min; "L": bright field; "R": red fluorescence image of **4** (λ_{ex} = 405 nm, λ_{em} = 547-647 nm), respectively.

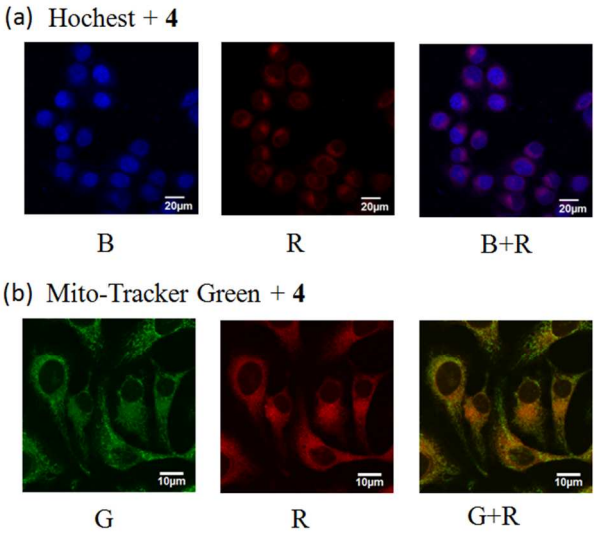

Figure 6. Co-localization imaging of the HeLa cells. Cells were pre-stained with (a) nucleus staining dye Hochest (10 mg/mL) or (b) Mito-Tracker Green (100 nM) for 20 min and then incubated with **4** (50 μM) for 10 min. "L": bright field; "B": blue fluorescence image of Hochest (λ_{ex} = 405 nm, λ_{em} = 420-480 nm); "G": green fluorescence image of Mito-Tracker Green (λ_{ex}=488 nm, λ_{em} = 500-540 nm); "R": red fluorescence image of **4** (λ_{ex} = 405 nm, λ_{em} = 550-650 nm), respectively.

Then co-localization experiments were performed to examine which subcellular location the probe stains. HeLa cells were firstly stained with Hochest (a nucleus stain, Figure 6a) or Mito-Tracker Green (a mitochondrial stain, Figure 6b), and then treated with the probe **4** (50 μM). Confocal microscopy analysis shows that the red fluorescence signal of probe **4** is well overlapped with the green fluorescence signal from the Mito-Tracker. Then the Pearson's correlation coefficient, used to quantify the overlap between the emission of **4** and Mito-Tracker, is further calculated as 0.86 (Figure S14), indicating that the probe shows good selectivity to mitochondria. The specifity is probably because some molecules of **4** (containing amino group) might undergo ionization to generate positive charges, which could bind to the mitochondrial membrane of negative potential[58-60].

CONCLUSION

A new red fluorescent molecule **1** with AIE and ESIPT characteristics was designed and synthesized. To prolong the emission wavelength of the AIE molecule salicyladazine, **1** incorporates diethylamino group as the electron donor and maleonitrile as the electron acceptor, thus making it exhibiting bright red fluorescence (λ_{em} = 650 nm, Φ_F = 24.3%) in the solid state. Interestingly, control compound **2** and **3**, which have similar structures as **1**, show obviously contrary characteristics (ACQ). The crystal analysis reveals that the interplanar spacing plays a decisive role for realizing the AIE characteristics of **1**. Moreover, a light-up fluorescent probe **4** was further developed for esterase activity detection by blocking the hydroxyl group of **1** with an esterase selective acetoxyl group. Upon the addition of esterase, the hydroxyl group of **4** was recovered, resulting in **1** with ESIPT and strong fluorescence in the aggregate states. The reaction product of **4** with esterase well accumulated in mitochondria of living cells and displayed strong emission due to its AIE characteristics, making **4** a good contrast agent for imaging mitochondrial esterase.

ASSOCIATED CONTENT

Supporting Information

Materials and instrumentation; absorption and fluorescence spectroscopic data of **1** in different organic solvents; effect of concentration and pH on the fluorescence of **1**, **2** and **3**; confirmation of the formation of **1** from **4** and esterase; NMR and MS results of compound **1**, **2**, **3**, **4**, co-localization imaging of HeLa cells; Z potential analysis of **4**; DLS analysis of **4** in the presence of esterase

Cif files of compound **1**, **2** and **3**

AUTHOR INFORMATION

Corresponding Authors

*E-mail: cheliub@nus.edu.sg. Fax: +65-67791936.

* Email: tongaj@mail.tsinghua.edu.cn. Fax: +86-10-62787682.

Notes

The authors declare no competing financial interest.

ACKNOWLEDGMENTS

We are very grateful for the financial support from the National Natural Science Foundation of China (Nos. 21375074, 21390410 and 21621003), Singapore National Research Foundation (R-279-000-444-281, R279-000-483-281), National University of Singapore (R279-000-482-133), the Institute of Materials Research and Engineering (IMRE/14-8P1110) and China Postdoctoral Science Foundation (2016M601000).

REFERENCES

1. Au-Yeung, H. Y.; Chan, J.; Chantarojsiri, T.; C. J. Chang, C. J. *J. Am. Chem. Soc.* **2013**, *135*, 15165-15173.
2. Chen, P.; He, C. *J. Am. Chem. Soc.* **2004**, *126*, 728-729.
3. Deng, R.; Xie, X.; Vendrell, M.; Chang, Y. T.; Liu, X. *J. Am. Chem. Soc.* **2011**, *133*, 20168-20171.
4. Feig, A. L.; Lippard, S. J. *Chem. Rev.* **1994**, *94*, 759-805.
5. Hayashita, T.; Qing, D.; Minagawa, M.; Lee, J. C.; Ku, C. H.; Teramae, N. *Chem. Commun.* **2003**, 2160-2161.
6. Kim, H. N; Ren, W. X.; Kim, J. S.; Yoon, J. *Chem. Soc. Rev.* **2012**, *41*, 3210-3244.
7. Li, X. H.; Gao, X. H.; Shi, W.; Ma, H. M. *Chem. Rev.* **2013**, *114*, 590-659.
8. Liu, J.; Cao, Z.; Lu, Y. *Chem. Rev.* **2009**, *109*, 1948-1998.
9. Yuan, L.; Lin, W. Y.; Zheng, K. B.; He, L. W.; Huang, W. M. *Chem. Soc. Rev.* **2013**, *42*, 622-661.
10. Kaur, M.; Choi, D. H. *Chem. Soc. Rev.* **2015**, *44*, 58-77.
11. Liu, H. W.; Zhang X. B.; Zhang, J.; Wang, Q. Q.; Hu, X. X.; Wang, P.; Tan, W. H. *Anal. Chem.* **2015**, *87*, 8896-8903.
12. Zhu, W.; Huang, X. M.; Guo, Z. Q.; Wu, X. M.; Yu, H. H.; Tian, H. *Chem. Commun.* **2012**, *48*, 1784-1786.
13. Birks, J. B. *Photophysics of Aromatic Molecules*, Wiley, New York, **1970**.
14. Thompson, R. B. *Fluorescence sensors and biosensors*, CRC Press, **2005**.
15. Johansson, M. K.; Cook, R. M. *Chemistry*, **2003**, *9*, 3466-3471.
16. Myochin, T.; Hanaoka, K.; Komatsu, T.; Terai, T.; Nagano, T. *J. Am. Chem. Soc.* **2012**, *134*, 13730-13737.
17. Chi, Z.; Zhang, X.; Xu, B.; Zhou, X.; Ma, C.; Zhang, Y.; Liu, S.; Xu, J. *Chem. Soc. Rev.* **2012**, *41*, 3878-3896.
18. Hong, Y.; Lam, J. W.; Tang, B. Z. *Chem. Soc. Rev.* **2011**, *40*, 5361-5388.
19. Mei, J.; Leung, N. L. C.; Kwok, R. T. K.; Lam, J. W. Y.; Tang, B. Z. *Chem. Rev.* **2015**, *115*, 11718-11940.
20. Yang, J.; Huang, J.; Sun, N.; Peng, Q.; Li, Q. Q.; Ma, D. G.; Li, Z. *Chem.- Eur. J.* **2015**, *21*, 6862-6868.
21. Zhan, X.; Wu, Z.; Lin, Y.; Xie, Y.; Peng, Q.; Li, Q.; Ma, D.; Li, Z. *Chem. Sci.* **2016**, *7*, 4355-4363.
22. Zhuang, Y.; Huang, F. J.; Xu, Q.; Zhang, M. S.; Lou, X. D.; Xia, F. *Anal. Chem.* **2016**, *88*, 3289-3294.
23. Zhang, M.; Feng, G.; Song, Z.; Zhou, Y. P.; Chao, H. Y.; Yuan, D.; Tan, T. T.; Guo, Z.; Hu, Z.; Tang, B. Z. *J. Am. Chem. Soc.* **2014**, *136*, 7241-7244.
24. Han, T. Y.; Feng, X.; Tong, B.; Shi, J. B.; Chen, L.; Zhi, J. G.; Dong, Y. P.; *Chem. Commun.* **2012**, *48*, 416-418.
25. Gui, S. L.; Huang, Y. Y.; Hu, F.; Jin, Y. L.; Zhang, G. X.; Yan, L. S.; Zhang, D. Q.; Zhao, R. *Anal. Chem.* **2015**, *87*, 1470-1474.
26. Niu, C. X.; You, Y.; Zhao, L.; He, D. C.; Na, N.; Ouyang, J. *Chem.-Eur. J.* **2015**, *21*, 13983-13990.
27. Wang, F. F.; Wen, J. Y.; Huang, L. Y.; Huang, J. J.; Ouyang, J. *Chem. Commun.* **2012**, *48*, 7395-7397.
28. Lu, H.; Zheng, Y.; Zhao, X.; Wang, L.; Ma, S.; Han, X.; Xu, B.; Tian, W.; Gao, H. *Angew. Chem. Int. Ed.* **2015**, *55*, 155-159.
29. Zhao, N.; Chen, S.; Hong, Y.; Tang, B. Z. *Chem. Commun.* **2015**, *51*, 13599-13602.
30. Hu, F.; Huang, Y. Y.; Zhang, G. X.; Zhao, R.; Yang. H.; Zhang, D. Q. *Anal. Chem.* **2014**, *86*, 7987-7995.
31. Shao, A.; Xie, Y.; Zhu, S.; Guo, Z.; Zhu, S.; Guo, J.; Shi, P.; James, T. D.; Tian, H.; Zhu, W. H. *Angew. Chem. Int. Ed.* **2015**, *54*, 7275-7280.
32. Ning, Z.; Chen, Z.; Zhang, Q.; Yan, Y. L.; Qian, S.; Cao, Y.; Tian, H. *Adv. Funct. Mater.* **2007**, *17*, 3799-3807.
33. Hang, Y. D.; Wang, J.; Jiang, T.; Lu, N. N.; Hua, J. L. *Anal. Chem.* **2016**, *88*, 1696-1703.
34. Chen, C. T. *Chem. Mater.* **2004**, *16*, 4389-4400.
35. Wang, Z.; Yan, L.; Lei, Z.; Chen, Y.; Hui, L.; Zhang, J.; Yan, Z.; Xing, L.; Xu, B.; Fu, X. *Polym. Chem.* **2014**, *5*, 7013-7020.
36. Tang, W. X.; Xiang, Y.; Tong, A. J. *J. Org. Chem.* **2009**, *74*, 2163-2166.
37. Hu, Q. L.; Gao, M.; Feng, G. X.; Liu, B. *Angew. Chem. Int. Ed.* **2014**, *53*, 14225-14229.
38. Lochbrunner, S.; Schultz, T.; Schmitt, M.; Shaffer, J.; Zgierski, M.; Stolow, A. *J. Chem. Phys.* **2001**, *114*, 2519-2522.
39. Mutai, T.; Sawatani, H.; Shida, T.; Shono, H.; Araki, K.; *J. Org. Chem.* **2013**, *78*, 2482-2489.
40. Peng, L.; Gao, M.; Cai, X. L.; Zhang, R. Y.; Li, K.; Feng, G. X.; Tong, A. J.; Liu, B. *J. Mater. Chem. B* **2015**, *3*, 9168-9172.
41. Peng, L.; Zheng, Y.; Wang, X. Y.; Tong, A. J.; Xiang, Y. *Chem.- Eur. J.* **2015**, *21*, 4326-4332.
42. Komatsu, T.; Urano, Y.; Fujikawa, Y.; Kobayashi, T.; Kojima, H.; Terai, T.; Hanaoka, K.; Nagano, T. *Chem. Commun.* **2009**, *45*, 7015-7017.
43. Levine, S. R.; Beatty, K. E. *Chem. Commun.* **2015**, *52*, 1835-1838.
44. Munoz-Torrero, D. *Curr. Med. Chem.* **2008**, *15*, 2433-2455.
45. Vandevoorde, S. *Curr. Top. Med. Chem.* **2008**, *8*, 247-267.
46. Lavis, L. D. *ACS Chem. Bio.* **2008**, *3*, 203-206.

47. Derikvand, F.; Yin, D. T.; Barret, R; Brumer, H. *Anal. Chem.* **2016**, *88*, 2989-2993.
48. Kim, S.; Kim, H.; Choi, Y.; Kim, Y. *Chem.- Eur. J.* **2015**, *21*, 9645-9649.
49. Gao, M.; Sim, C. K.; Leung, C. W. T.; Hu, Q.; Feng, G. X.; Xu, F.; Tang, B. Z.; Liu, B. *Chem. Commun.* **2014**, *50*, 8312-8315.
50. Hao, Z.; Fan, J.; Du, J.; Peng, X. J. *Accounts Chem. Res.* **2016**, *49*, 2115-2126.
51. Wallace, D. C. *Science* **1999**, *283*, 1482-1488.
52. Tang, B. Z.; Geng, Y.; Lam, J. W. Y.; Li, B.; Jing, X.; Wang, X.; Wang, F.; Pakhomov, A. B.; Zhang, X. X. *Chem. Mater.* **1999**, *11*, 1581-1589.
53. Ren, Y.; Lam, J. W. Y.; Dong, Y. Q.; Tang, B. Z.; Wong, K. S. *J. Phys. Chem. B* **2005**, *109*, 1135-1140.
54. Wang, Y. J.; Shi, Y.; Wang, Z.; Zhu, Z.; Zhao, X.; Nie, H.; Qian, J.; Qin, A.; Sun, J. Z.; Tang, B. Z. *Chem.- Eur. J.* **2016**, *22*, 9784-9791..
55. Wang, X. H.; Guo, Z. Q.; Zhu, S. Q.; Liu, Y. J.; Shi, P.; Tian, H.; Zhu, W. H. *J. Mater. Chem. B* **2016**, *4*, 4683-4689.
56. Han, T. Y.; Hong, Y. N.; Xie, N.; Chen, S. J.; Zhao, N.; Zhao, E. G.; Lam, J. W. Y.; Sung, H. H. Y.; Dong, Y. P.; Tong, B.; Tang, B. Z. *J. Mater. Chem. C* **2013**, *1*, 7314-7320.
57. Kosower, E. M.; Dodiuk, H.; Kanety, H. *J. Am. Chem. Soc.* **1978**, *100*, 4179-4188.
58. Chevalier, A.; Zhang, Y.; Khdour, O. M.; Kaye, J. B.; Hecht, S. M. *J. Am. Chem. Soc.*, **2016**, *138,* 12009-12012.
59. Yousif, L. F.; Stewart, K. M.; Kelley, S. O. *ChemBioChem*, **2009**, *10*, 9-10.
60. Zhang, G.; Sun, Y. M.; He, X. Q.; Zhang, W. J.; Tian, M. G.; Feng, R. Q.; Zhang, R. Y.; Li, X. C.; Guo, L. F.; Yu, X. Q.; Zhang, S. L. *Anal. Chem.* **2015**, *87*, 12088-12095.

For TOC only

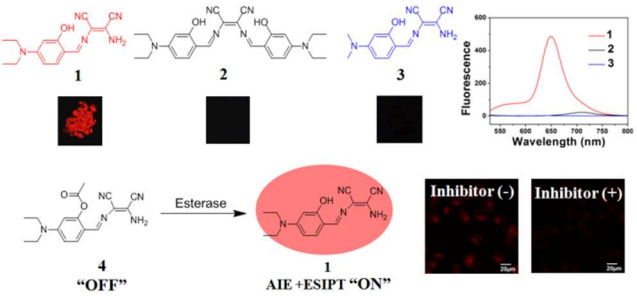
1
2
3
Fluorescence
Wavelength (nm)
Esterase
4
"OFF"
1
AIE +ESIPT "ON"
Inhibitor (-)
Inhibitor (+)